Pure appl. geophys. 163 (2006) 175–207
0033–4553/06/010175–33
DOI 10.1007/s00024-005-0002-1

Pure and Applied Geophysics

Physics and Seismic Modeling for Monitoring CO_2 Storage

José M. Carcione,[1] Stefano Picotti,[1] Davide Gei,[1] and Giuliana Rossi[1]

Abstract—We present a new petro-elastical and numerical-simulation methodology to compute synthetic seismograms for reservoirs subject to CO_2 sequestration. The petro-elastical equations model the seismic properties of reservoir rocks saturated with CO_2, methane, oil and brine. The gas properties are obtained from the van der Waals equation and we take into account the absorption of gas by oil and brine, as a function of the *in situ* pore pressure and temperature. The dry-rock bulk and shear moduli can be obtained either by calibration from real data or by using rock-physics models based on the Hertz-Mindlin and Hashin-Shtrikman theories. Mesoscopic attenuation due to fluids effects is quantified by using White's model of patchy saturation, and the wet-rock velocities are calculated with Gassmann equations by using an effective fluid modulus to describe the velocities predicted by White's model. The simulations are performed with a poro-viscoelastic modeling code based on Biot's theory, where viscoelasticity is described by generalizing the solid/fluid coupling modulus to a relaxation function. Using the pseudo-spectral method, which allows general material variability, a complete and accurate characterization of the reservoir can be obtained. A simulation, that considers the Utsira sand of the North Sea, illustrates the methodology.

Key words: CO_2 sequestration, rock physics, seismic modeling, storage, monitoring.

Introduction

Fossil-fuel combustion generates in excess of 27 billion tons of carbon dioxide (CO_2) per year, which is mainly discharged into the atmosphere. There is evidence that this concentration of CO_2 has increased the atmosphere temperature by 0.3–0.6°C during the last 150 years (Ledley *et al.*, 1999). To solve this problem, geological sequestration is an immediate option. The possibilities are injection into hydrocarbon reservoirs, methane-bearing coal beds and saline aquifers. An example of the latter is the Sleipner field in the North Sea (Arts *et al.*, 2004), where CO_2 is stored in the Utsira formation, a highly permeable porous sandstone 800 m below the sea bottom (Færseth, 1996; Carcione and Tinivella, 2001). Carbon dioxide stored in saline aquifers has some advantages, because it does not require structural

[1]Istituto Nazionale di Oceanografia e di Geofisica Sperimentale (OGS), Borgo Grotta Gigante 42c, 34010, Sgonico, Trieste, Italy. E-mail: jcarcione@ogs.trieste.it

and stratigraphic trap geometries. The storage can be hydrodynamic as dissolved CO_2 in the formation waters. However, the disposal should be made at supercritical pressures to avoid the presence of the gas phase, with the minimum aquifer depth of nearly 1 km (the critical pressure and temperature of CO_2 are 7.4 MPa and 31°C, respectively).[1] As noted by OLDENBURG (2003), the density change of CO_2 is large in the transition from gaseous to supercritical conditions, and can approach that of liquid water. Instead, pure CH_4 (methane, hydrocarbon gas) exhibits no such drastic change. Also, the viscosity of CO_2 is low but always higher than the CH_4 viscosity.

The effects of pore pressure on the frame of the host rock and the contrast between the acoustic properties of oil and brine and those of CO_2 are the main factors to detect and monitor the presence of CO_2. WANG *et al.* (1998) measured a pore pressure increase from 8 to 16 MPa due to CO_2 flooding at the McElroy field in West Texas. XUE and OHSUMI (2004) performed laboratory experiments and measured a P-wave velocity change of 6% caused by gaseous CO_2 injection and 10% due to supercritical CO_2 injection. Moreover, there may be reactions with native minerals, particularly the generation of carbonates (KASZUBA *et al.*, 2003). PREUSS *et al.* (2001) found that the amount of CO_2 that may be sequestered by precipitation of secondary carbonates (mainly calcite and dolomite) is comparable to the amount of CO_2 dissolved in pore waters. In this case, the generation of carbonates may increase the dry-rock moduli by increasing cementation and decreasing porosity. These variations may indicate that seismic methods can be used to detect and monitor the presence and movement of carbon dioxide in the subsurface.

Firstly, we define the fluid properties as a function of pressure and temperature, with the gas acoustic properties obtained from the real-gas van der Waals equation. We take into account the possibility that CH_4 and CO_2 can go into solution in the oil and brine. This process affects the saturation of the gaseous phases and the density and bulk moduli of the liquid phases. Secondly, we obtain the dry-rock moduli as a function of effective pressure, being the main acoustic properties affected by pore pressure changes. The wet-rock moduli and velocities are obtained by using Gassmann's equations, and the seismic modeling (synthetic seismograms) is based on Biot's theory of poroelasticity, including attenuation described by viscoelasticity and White's model of patchy saturation (e.g, MAVKO *et al.*, 1998; CARCIONE, 2001). The poro-viscoelastic equations are solved with an algorithm developed by CARCIONE and HELLE (1999), which uses a fourth-order Runge-Kutta time-stepping scheme and the staggered Fourier method for computing the spatial derivatives.

[1] 1 MPa = 10 bar = 145.04 psi = 9.87 atm.

Acoustic Properties of the Fluids

The properties of the fluids involved in the sequestration process (CO_2, hydrocarbon gas, oil, and brine) depend on temperature and pressure, which in turn depend on depth z. A simple (reference) situation is to consider a constant geothermal gradient, G, such that the temperature variation with depth is

$$T = T_0 + Gz, \tag{1}$$

where T_0 is the surface temperature (typical values of G range from 20 to 30°C/km). The pore pressure p at depth z depends on many factors, most of them of geological nature, such as low-permeability regions, sealing faults and hydrocarbons caps, which prevent pressure equilibration (communication) from the reservoir to the surface. The simplest case is when there are no permeability barriers and the fluid (say, water) is free to flow from depth z to the surface. In this case, the pore pressure is hydrostatic and is given by

$$p = \rho_w g z, \tag{2}$$

where ρ_w is the water density and g is the acceleration of gravity. With $\rho_w = 1\text{g/cm}^3$, the pore pressure ranges from 0 MPa at the surface to 30 MPa at 3 km depth.

Properties of Hydrocarbon Gas and CO_2

In situ reservoir gas behaves as a real gas, which satisfies approximately the van der Waals equation (FRIEDMAN, 1963):

$$(p + a\rho_g^2)(1 - b\rho_g) = \rho_g R(T + 273), \tag{3}$$

where p is the gas pressure, ρ_g is the gas density and $R = 8.31$ J/(mol °K) is the gas constant.

For CO_2, $a = 0.359$ (Pa m^3/mole)^2 = 185.43 Pa (m^3/kg)^2 and $b = 42.7$ cm^3/mole $= 0.97 \times 10^{-3}$ m^3/kg (one mole of CO_2 corresponds to 44 g). The critical pressure and temperature are 7.4 MPa and 31°C, respectively. For CH_4, $a = 0.225$ Pa (m^3/mole)^2 = 879.9 Pa (m^3/kg)^2 and $b = 42.7$ cm^3/mole $= 2.675 \times 10^{-3}$ m^3/kg (one mole of methane corresponds to 16 g). The critical pressure and temperature are 4.6 MPa and −82.7°C, respectively. Equation (3) gives the gas density as a function of pressure and temperature which can be related to depth, if we assume that the gas pressure is equal to the expected formation pressure.

The isothermal gas compressibility c_T depends on pressure. It can be calculated from the van der Waals equation using

$$c_T = \frac{1}{\rho_g}\frac{\partial \rho_g}{\partial p}, \tag{4}$$

which gives

$$c_T = \left[\frac{\rho_g R(T+273)}{(1-b\rho_g)^2} - 2a\rho_g^2\right]^{-1}. \tag{5}$$

For sound waves below 1 GHz or so, it is a better approximation to assume that the compression is adiabatic, i.e., that the entropy content of the gas remains nearly constant during the compression (MORSE and INGARD, 1986). Adiabatic compressibility c_S is related to isothermal compressibility c_T by $c_S = c_T/\gamma$, where γ is the heat capacity ratio at constant pressure, which depends on measurable quantities (MORSE and INGARD, 1986). For polyatomic gases we may use the approximation $\gamma \approx 4/3$. In this case, the gas bulk modulus can be expressed as

$$K_g = \frac{1}{c_S} = \frac{4}{3c_T}. \tag{6}$$

It can be shown that equation (3) can be a good approximation to the behavior of natural gas and carbon dioxide (i.e., multi-component gases), since the differences between the experimental data — as represented by Standing's results (STANDING, 1952) — and the van der Waals results are only about 15% over the depths of interests. Alternative expressions for the acoustic properties of gases can be found in BATZLE and WANG (1992) and SPAN and WAGNER (1996).

Properties of Oil and Brine

The liquid properties depend on temperature and pressure, and on API number and salinity, if the fluid is oil or water, respectively. BATZLE and WANG (1992) and MAVKO *et al.* (1998, pp. 214–220) provide a series of useful empirical relations between the state variables and velocity and density. For completeness we state these relations here. The equations are limited to the pressures and temperatures of the experiments made by BATZLE and WANG (1992) (around 60 MPa and 100°C).

Oil density (in g/cm^3) versus temperature T (in °C) and pressure p (in MPa) can be expressed as

$$\rho_o = \frac{\rho_0 + (0.00277p - 1.71\times10^{-7}p^3)(\rho_0 - 1.15)^2 + 3.49\times10^{-4}p}{0.972 + 3.81\times10^{-4}(T+17.78)^{1.175}}, \tag{7}$$

where ρ_0 is the density at 15.6°C and atmospheric pressure. This density is related to API gravity by

$$\text{API} = \frac{141.5}{\rho_0} - 131.5. \tag{8}$$

The expression relating wave velocity of dead oil (oil with no dissolved gas) to pressure, temperature and API gravity is

$$V_o = 15450(77.1 + \text{API})^{-1/2} - 3.7\,T + 4.64p + 0.0115(0.36\ \text{API}^{1/2} - 1)Tp, \tag{9}$$

where V_o is given in m/s and p in MPa. Using these relationships, we obtain the oil bulk modulus as $K_o = \rho_o V_o^2$.

The density of brine in g/cm^3 is given by

$$\begin{aligned}\rho_B = \rho_w + S\{&0.668 + 0.44S + 10^{-6} \\ &[300p - 2400pS + T(80 + 3T - 3300S - 13p + 47pS)]\},\end{aligned} \tag{10}$$

with

$$\begin{aligned}\rho_w = 1 + 10^{-6}\big(&- 80T - 3.3T^2 + 0.00175T^3 + 489p - 2Tp \\ &+ 0.016T^2p - 1.3 \times 10^{-5}T^3p - 0.333p^2 - 0.002Tp^2\big),\end{aligned} \tag{11}$$

where S is the weight fraction (ppm/1000000) of sodium chloride. Finally, the velocity function for brine is

$$\begin{aligned}V_B = V_w &+ S(1170 - 9.6T + 0.055T^2 - 8.5 \times 10^{-5}T^3 + 2.6p - 0.0029Tp - 0.0476p^2) \\ &+ S^{1.5}(780 - 10p + 0.16p^2) - 1820S^2,\end{aligned} \tag{12}$$

where V_w is the velocity of pure water given by

$$V_w = \sum_{i=0}^{4}\sum_{j=0}^{3} w_{ij}T^i p^j, \tag{13}$$

with constants w_{ij} given in Table 1. The same units, introduced before, are used here and in the rest of the paper. Using these relationships, we get the brine bulk modulus as $K_B = \rho_B V_B^2$.

Gas Absorbed by Oil and Brine

Part of the hydrocarbon gas and CO_2 can dissolve in oil and the rest remains as free gas. This process generates live oil, which has different properties of the original (dead) oil. The process is illustrated in Figure 1. The injected gas displaces part of the

Table 1
Coefficients for water-properties calculation

$w_{00} = 1402.85$	$w_{02} = 3.437 \times 10^{-3}$
$w_{10} = 4.871$	$w_{12} = 1.739 \times 10^{-4}$
$w_{20} = -0.04783$	$w_{22} = -2.135 \times 10^{-6}$
$w_{30} = 1.487 \times 10^{-4}$	$w_{32} = -1.455 \times 10^{-8}$
$w_{40} = -2.197 \times 10^{-7}$	$w_{42} = 5.230 \times 10^{-11}$
$w_{01} = 1.524$	$w_{03} = -1.197 \times 10^{-5}$
$w_{11} = -0.0111$	$w_{13} = -1.628 \times 10^{-6}$
$w_{21} = 2.747 \times 10^{-4}$	$w_{23} = 1.237 \times 10^{-8}$
$w_{31} = -6.503 \times 10^{-7}$	$w_{33} = 1.327 \times 10^{-10}$
$w_{41} = 7.987 \times 10^{-10}$	$w_{43} = -4.614 \times 10^{-13}$

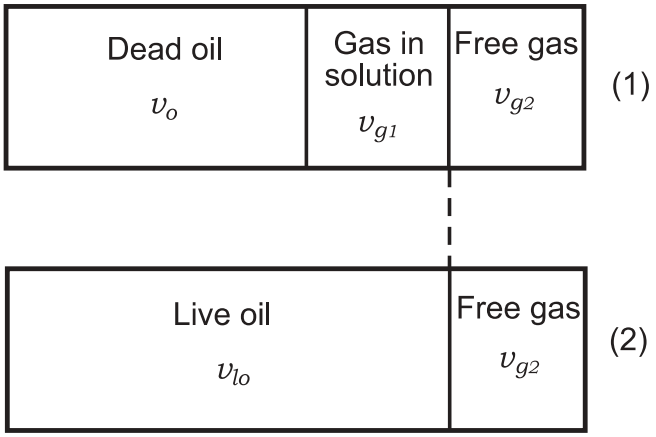

Figure 1
Absorption of gas by dead oil.

dead oil, such that at stage 1 there is a gas volume $v_g = v_{g1} + v_{g2}$, with v_{g1} going immediately into solution and v_{g2} remaining as free gas (stage 2).

The volume ratio of liberated gas to remaining oil at atmospheric pressure and 15.6°C is

$$R_G = 2.03\ G_r[p\exp(0.02878\ \text{API} - 0.00377\ T)]^{1.205}, \tag{14}$$

where G_r is the hydrocarbon gas or CO_2 gravity (0.56 and 1.51, respectively); R_G, given in liters of gas/liters of oil, represents the maximum amount of gas that can be dissolved in the oil (BATZLE and WANG, 1992). Although R_G corresponds to pressure p and temperature T, it is given at atmospheric conditions. From a mass balance, the equivalent ratio at depth z is

$$R'_G = \left(\frac{\rho_{gs}}{\rho_g}\right)\left(\frac{\rho_o}{\rho_{os}}\right)R_G = \frac{v_{g1}}{v_o} \tag{15}$$

where ρ_{gs}, ρ_{os} and ρ_g, ρ_o are the gas and oil densities at the surface and at depth z, respectively, and v_o is the volume of dead oil. The gas densities can be computed from the van der Waals equation (3).

Let us now obtain the properties of the liquid-gas mixture considering absorption of gas by the liquid. First, let us assume that the oil has absorbed the maximum amount of gas, i.e., there is free gas in the pore space. The saturation of gas *before* the absorption (stage 1) is equal to

$$S_g = \frac{v_g}{v_o + v_g}, \tag{16}$$

where $v_g = v_{g1} + v_{g2}$ (see Fig. 1). A critical saturation S_{gc} can be obtained when $v_{g2} = 0$, or $v_g = v_{g1}$; from equation (16), $v_g = v_o S_g/(1 - S_g)$, and using equation (15), we obtain

$$S_{gc} = \frac{R'_G}{1 + R'_G}. \tag{17}$$

When $S_g \geq S_{gc}$, part of the gas is dissolved in the oil and the rest is in the form of free gas. In this case, the oil absorbs the maximum quantity of gas. It can be shown by using equation (16) that *after* the absorption, the final free-gas saturation (i.e., $v_{g2}/(v_{g2} + v_o)$) is given by

$$s_g = \frac{S_g - S_{gc}}{1 - S_{gc}}, \quad S_g \geq S_{gc}. \tag{18}$$

The sound velocity of the saturated live oil, V_{los}, is calculated by using a pseudo-density ρ' based on the expansion caused by gas intake,

$$\rho' = \frac{\rho_0}{B_0}(1 + 0.001\ R_G)^{-1} \tag{19}$$

(BATZLE and WANG, 1992). In order to obtain V_{los}, the density ρ_0 should be substituted by ρ' in equations (8) and (9). Then, the live-oil bulk modulus is $K_{los} = \rho_{lo} V_{los}^2$, where

$$\rho_{lo} = \rho_G + (0.00277p - 1.71 \times 10^{-7} p^3)(\rho_0 - 1.15)^2 + 3.49 \times 10^{-4} p, \tag{20}$$

$$\rho_G = (\rho_0 + 0.0012\ G_r R_G)/B_0 \tag{21}$$

is the saturation density, and

$$B_0 = 0.972 + 0.00038\left[2.4\ R_G\left(\frac{G_r}{\rho_0}\right)^{1/2} + T + 17.8\right]^{1.175} \tag{22}$$

is the oil volume factor (BATZLE and WANG, 1992).[2]

When $S_g < S_{gc}$, all the gas goes into solution, but the oil is not saturated since it absorbs less than R'_G liters of gas; it absorbs $(S_g/S_{gc})R'_G$. In this case, the velocity V_{lo} of live oil is obtained by substituting R_G by $(S_g/S_{gc})R_G$ in equations (19) and (9). The bulk modulus is $K_{lo} = \rho_{lo} V_{lo}^2$, where ρ_{lo} is given by equation (20), with R_G replaced by $(S_g/S_{gc})R_G$ in equations (21) and (22).

The amount of gas that can be dissolved in brine is much less than that in light oils. For temperatures below 250°C, the maximum amount of dissolved methane (at room pressure and temperature) is

[2]When computing the density of live oil, the temperature effect was considered twice in BATZLE and WANG (1992): in B_0 and in their equation (19) (M. Batzle, personal communication). Equation (20) gives the correct density.

$$\log_{10}(R_G) = \log_{10}\{0.712p|T - 76.71|^{1.5} + 3676p^{0.64}\} - 4 - 7.786S(T + 17.78)^{-0.306} \tag{23}$$

(BATZLE and WANG, 1992). As before, we consider the equivalent ratio R'_G, so that

$$R'_G = \left(\frac{\rho_{gs}}{\rho_g}\right)\left(\frac{\rho_w}{\rho_{ws}}\right)R_G, \tag{24}$$

where ρ_{ws} and ρ_w are the density of water at the surface and depth z, respectively. This defines a critical saturation (17) and a real saturation (18).

Recent experimental data indicate that gas in solution in brine has no effect on the bulk modulus (M. Batzle, personal communication). To obtain the brine density with dissolved gas, we note that the maximum dissolved-gas mass per unit volume at depth z is $\rho_g R'_G$. Then, the correction to the brine density is

$$\begin{aligned} &\rho_B \rightarrow \rho_B + \rho_g R'_G, && S_g > S_{gc}, \\ &\rho_B \rightarrow \rho_B + \rho_g R'_G\left(\frac{S_g}{S_{gc}}\right), && S_g \leq S_{gc}. \end{aligned} \tag{25}$$

We assume the same equations for CH_4 and CO_2.

Effective Fluid Model

The mixture of gas (CH_4 or CO_2) with live oil or brine behaves as a composite fluid with properties depending on the stiffness moduli of the constituents and their respective saturations, s_g and s_l, where l – denoting "liquid" – refers either to live oil or to brine. We obtain the properties of the gas-liquid mixture by using Wood's model (MAVKO *et al.*, 1998). The bulk modulus is

$$K_f = (s_g K_g^{-1} + s_l K_l^{-1})^{-1}, \tag{26}$$

where $s_l = 1 - s_g$.

When the fluids are not mixed in the pore volume, but distributed in patches, the effective bulk modulus of the fluid at high frequencies is higher than that predicted by Wood's model. To obtain the bulk modulus of the gas-liquid mixture, we use an empirical law introduced by BRIE *et al.* (1995). The effective bulk modulus is given by

$$K_f = (K_l - K_g)s_l^e + K_g, \tag{27}$$

where e is an empirical parameter This equation fits data from the seismic to the ultrasonic band, particularly, the sonic-band values provided by BRIE *et al.* (1995). Equation (27) gives Voigt's mixing law for $e = 1$ and an approximation to Wood's model for $e = 40$. In order to quantify the exponent e on physical ground, we use White's model of patchy saturation (WHITE, 1975; MAVKO *et al.*, 1998; CARCIONE *et al.*, 2003a,b). It is assumed that the medium has patches of CO_2 in a brine

saturated background, where brine has absorbed the maximum amount of CO_2. White's model describes wave velocity and attenuation as a function of frequency, patch size, permeability and viscosity. Attenuation and velocity dispersion is caused by fluid flow between patches of different pore pressures. The critical fluid diffusion relaxation scale is proportional to the square-root of the ratio permeability to frequency. At seismic frequencies the length scale is very large, and the pressure is nearly uniform throughout the medium, however as frequency increases, pore pressure differences can cause an important increase in P-wave velocity (see the appendix).

The density of the gas-liquid mixture is simply

$$\rho_f = s_g \rho_g + s_l \rho_l. \tag{28}$$

For modeling purposes, the fluid viscosity of the mixture is

$$\eta_f = \eta_g \left(\frac{\eta_l}{\eta_g} \right)^{s_l} \tag{29}$$

(TEJA and RICE, 1981). The viscosity of oil and brine is obtained by using the equations given in BATZLE and WANG (1992). We also make use of the book by POLING *et al.* (2001), in which the properties of gases and liquids are given in detail. No dependence of viscosity versus dissolved-gas content is assumed.

Dry-Rock Bulk and Shear Moduli

The behavior of the dry frame (or skeleton) as a function of the confining and pore pressures is a key acoustic property of the rock. The dry-rock moduli as a function of depth and pressure are assumed to have the following general form

$$K_m(p_e) = a_0 + a_1 p_e + a_2 \exp(-p_e/p_K) \tag{30}$$

and

$$\mu_m(p_e) = b_0 + b_1 p_e + b_2 \exp(-p_e/p_\mu) \tag{31}$$

(e.g., PRASAD and MANGHNANI, 1997; CARCIONE and TINIVELLA, 2001; KASELOW and SHAPIRO, 2004), where a_i, b_i, p_K and p_μ are constants and $p_e = p_c - np$ is the effective pressure, with p_c the confining pressure and n the effective-stress coefficient. K_m and μ_m have different coefficients; let us denote them by n_K and n_μ, respectively. In theory, these coefficients are equal to 1 for the dry-rock moduli (ZIMMERMAN, 1991, p. 43; CARCIONE, 2001, p. 233), although under real conditions this value may not be appropriate and calibration becomes necessary (e.g., GEI and CARCIONE, 2003). The lithostatic or confining pressure p_c can be obtained by integrating the density log as

$$p_c = g \int_0^z \rho(z')\, dz', \tag{32}$$

where ρ is the density of the overburden. The parameters in equations (30) and (31) are obtained by calibration with sonic-log or laboratory data, as we shall see below. Controlled laboratory experiments allow a precise determination of n_k and n_μ, while we assume that these coefficients are equal to one when using sonic-log velocities. Another alternative is to use theoretical models, such as the Hertz-Mindlin model (e.g., MAVKO *et al.*, 1998) (see below).

Grain Properties

The presence of clay, calcite, dolomite, etc., modifies the effective bulk modulus of the grains. That is, the grains are formed by a mixture of quartz and other $n-1$ solids. We assume that K_s and μ_s are equal to the arithmetic average of the upper and lower Hashin-Shtrikman bounds (HASHIN and SHTRIKMAN, 1963). Defining the solid fractions by ϕ_i, the following relation hold

$$\phi + \sum_{i=1}^{n} \phi_i = 1. \tag{33}$$

The Hashin-Shtrikman upper (+) and lower (−) bounds for the bulk and shear moduli are

$$\begin{aligned} K^{\mathrm{HS}\pm} &= \Lambda(\mu_\pm), \\ \mu^{\mathrm{HS}\pm} &= \Gamma[\xi(K_\pm, \mu_\pm)], \end{aligned} \tag{34}$$

where

$$\Lambda(\mu_\pm) = \left\langle \frac{1}{K + \frac{4}{3}\mu_\pm} \right\rangle^{-1} - \frac{4}{3}\mu_\pm, \tag{35}$$

$$\Gamma(\xi) = \left\langle \frac{1}{\mu + \xi} \right\rangle^{-1} - \xi, \tag{36}$$

$$\xi(K_\pm, \mu_\pm) = \frac{\mu_\pm}{6}\left(\frac{9K_\pm + 8\mu_\pm}{K_\pm + 2\mu_\pm}\right) \tag{37}$$

(e.g., MAVKO *et al.*, 1998), and the subscripts + and − denote the maximum and minimum moduli of the single constituents. The brackets $\langle\cdot\rangle$ indicate an average over the constituents weighted by their volume fractions. The density is simply the arithmetic average of the densities of the single constituents weighted by the corresponding volume fractions.

Calibration with Laboratory Data

The parameters in equations (30) and (31) can be obtained from experiments on dry samples by fitting the dry-rock moduli as a function of confining pressure, while n_K and n_μ are obtained from experiments on saturated samples for different confining and pore pressures (e.g., PRASAD and MANGHNANI, 1997; CARCIONE and GANGI, 2000; GEI and CARCIONE, 2003). If $V_P(\text{dry})$ and $V_S(\text{dry})$ are the experimental compressional and shear velocities, the moduli are approximately given by

$$K_m = (1-\phi)\rho_s\left(V_P(\text{dry})^2 - \frac{4}{3}V_S(\text{dry})^2\right)$$

and

$$\mu_m = (1-\phi)\rho_s V_S(\text{dry})^2, \tag{38}$$

where ϕ is the porosity and ρ_s is the grain density. We recall that K_m is the rock modulus at constant pore pressure, i.e., the case when the bulk modulus of the pore fluid is negligible compared with the dry-rock bulk modulus, as for example air at room conditions. Then, we perform experiments on saturated samples for different confining and pore pressures, to obtain the effective stress coefficients n_K and n_μ. Because these experiments yield the P- and S-wave velocities, and the effective stress coefficients of wave velocity and wave moduli may differ from each other, we obtain n_K and n_μ for the undrained (wet-rock) moduli

$$K = \rho\left(V_P^2 - \frac{4}{3}V_S^2\right) \quad \text{and} \quad \mu = \rho V_S^2. \tag{39}$$

Having obtained all the constants, we replace p_c by p_e in the expressions of the dry-rock moduli, to obtain them as a function of the confining and pore pressures.

Calibration with Sonic-log Data

The calibration with sonic-log data is less accurate than the calibration with laboratory data. Firstly, it is difficult to evaluate the effective-stress coefficients. We assume the theoretical values $n_K = n_\mu = 1$ and take $a_1 = b_1 = 0$ in equations (30) and (31). The dry-rock moduli K_m and μ_m are estimated from those parts of the sonic-log profile where there is full water saturation. We use the inverse Gassmann's equation to obtain the bulk modulus at different calibration points:

$$K_m = \frac{(\phi K_s/K_w + 1 - \phi)K - K_s}{\phi K_s/K_w + K/K_s - 1 - \phi} \tag{40}$$

(e.g., CARCIONE, 2001, p. 225; GEI and CARCIONE, 2003), where $K = \rho V_P^2 - (4/3)\mu$ is the wet-rock modulus and K_s is the bulk modulus of the grains. The dry-rock moduli is assumed to vary with depth as

$$K_m = K_\infty - (K_\infty - K_0)\exp(-p_d/p_K) \tag{41}$$

and

$$\mu_m = \mu_\infty - (\mu_\infty - \mu_0)\exp(-p_d/p_\mu), \tag{42}$$

where $p_d = p_c - p$ is the differential pressure, assuming that the pore pressure is that given by the drilling plan. The parameters are computed by fitting the sonic-log moduli at the calibration points.

Theoretical Model

In the absence of calibration data, the classical model to obtain the dry-rock moduli as a function of the effective (differential) pressure is the Hertz-Mindlin contact theory, that considers spherical grains. The moduli at the critical porosity are given by

$$K_{mc} = \left[\frac{C^2(1-\phi_c)^2\mu_s^2 p_d}{18\pi^2(1-\nu_s)^2}\right]^{1/3} \tag{43}$$

and

$$\mu_{mc} = \frac{5-4\nu_s}{5(2-\nu_s)}\left[\frac{3C^2(1-\phi_c)^2\mu_s^2 p_d}{2\pi^2(1-\nu_s)^2}\right]^{1/3} \tag{44}$$

(e.g., MAVKO *et al.*, 1998), where μ_s is the shear modulus of the grains, ν_s is the Poisson ratio of the grains, ϕ_c is the critical porosity and C is the average number of contacts per spherical grain. The critical porosity is the porosity above which the moduli are very small, i.e., the rock becomes a liquid suspension ($\phi_c = 0.36$ for a random dense pack of identical spherical grains). An approximate equation for C, based on Murphy's data (MURPHY, 1982), is $C = 2.8/\phi_c$.

Walton (WALTON, 1987; MAVKO *et al.*, 1998) obtained a model for infinitely rough spheres and ideally smooth spheres. The first is identical to the Hertz-Mindlin model described above, and the second has the same bulk modulus of the Hertz-Mindlin model but a different shear modulus, namely,

$$\mu_{mc} = \frac{3}{5}K_{mc} \tag{45}$$

(note that this relation corresponds to a Poisson solid).

To obtain the dry-rock moduli, we may use different models depending on whether the rock is consolidated or unconsolidated. In the first case, we use a Hill average, i.e., an arithmetic average of the Voigt and Wood moduli:

$$K_m = \frac{1}{2}(K_V + K_W) \quad \text{and} \quad \mu_m = \frac{1}{2}(\mu_V + \mu_W), \tag{46}$$

where

$$K_V = (1 - \phi/\phi_c)K_s + (\phi/\phi_c)K_{mc}, \quad \frac{1}{K_W} = \frac{(1 - \phi/\phi_c)}{K_s} + \frac{\phi\phi_c}{K_{mc}}, \tag{47}$$

$$\mu_V = (1 - \phi/\phi_c)\mu_s + (\phi/\phi_c)\mu_{mc} \quad \text{and} \quad \frac{1}{\mu_W} = \frac{(1 - \phi/\phi_c)}{\mu_s} + \frac{\phi/\phi_c}{\mu_{mc}}. \tag{48}$$

For unconsolidated rocks, we use the modified Hashin-Shtrikman lower bound introduced by DVORKIN and NUR (1996), and used by HOVERSTEN *et al.* (2003) to describe the effective dry-rock moduli of CO_2 bearing rocks. In this case,

$$K_m = \Lambda(\mu_{mc}) \tag{49}$$

and

$$\mu_m = \Gamma[\xi(K_{mc}, \mu_{mc})] \tag{50}$$

(see equations (35) and (36)), where, as above, the mineral grain — defined by K_s and μ_s — has a fraction $1 - \phi/\phi_c$ and the dry rock, defined by the critical moduli, has a fraction ϕ/ϕ_c.

Wet-Rock Compressional- and Shear-Wave Velocities

The low-frequency bulk modulus of the wet rock is given by Gassmann modulus

$$K = K_m + \alpha^2 M, \tag{51}$$

where

$$\alpha = 1 - \frac{K_m}{K_s} \quad \text{and} \quad M = \left(\frac{\alpha - \phi}{K_s} + \frac{\phi}{K_f}\right)^{-1} \tag{52}$$

(e.g., CARCIONE, 2001, p. 225). The shear modulus of the wet rock is simply the modulus of the dry rock, $\mu = \mu_m$. The P-wave and S-wave velocities (at low frequencies) are then

$$V_P = \sqrt{\frac{K + 4\mu/3}{\rho}} \quad \text{and} \quad V_S = \sqrt{\frac{\mu}{\rho}}, \tag{53}$$

where ρ is the bulk density, given by

$$\rho = (1 - \phi)\rho_s + \phi\rho_f. \tag{54}$$

An alternative model to obtain the Gassmann modulus has been developed by CARCIONE *et al.* (2005), who obtained the generalized modulus for a multi-phase system consisting of n solids and a saturating fluid. Let us define the fraction of solid i

by ϕ_i, such that satisfies equation (33), and the bulk modulus of solid i by K_i. The bulk modulus is then given by

$$K = \sum_{i=1}^{n} K_{mi} + \left(\sum_{i=1}^{n} \alpha_i \right)^2 M, \tag{55}$$

where

$$\alpha_i = \beta_i - \frac{K_{mi}}{K_i}, \tag{56}$$

$$M = \left(\sum_{i=1}^{n} \frac{\alpha_i - \beta_i \phi}{K_i} + \frac{\phi}{K_f} \right)^{-1} \tag{57}$$

and

$$\beta_i = \frac{\phi_i}{1 - \phi}. \tag{58}$$

The dry-rock modulus of each solid phase is given by a modified Krief model:

$$K_{mi} = (K_{\mathrm{HS}}/v)\beta_i K_i (1 - \phi)^{A/(1-\phi)}, \quad i = 1, \ldots, n, \tag{59}$$

where A is a dimensionless parameter, $v = \sum_{i=1}^{n-1} \beta_i K_i$ is the Voigt average, and $K_{\mathrm{HS}} = (K^{\mathrm{HS}+} + K^{\mathrm{HS}-})/2$, where $K^{\mathrm{HS}+}$ and $K^{\mathrm{HS}-}$ are the Hashin-Shtrikman (HS) upper and lower bounds given by equation (34). In order to include the pressure dependence, we assume that the porosity is given by

$$\phi = \phi_0 \exp(-p_d/p_\phi) \tag{60}$$

(ATHY, 1930), where ϕ_0 is the porosity at zero differential pressure, for instance, the rock at room conditions, and p_ϕ is a constant. Note that β_i should be constant for variations of the differential pressure.

Numerical Seismic Modeling

We use a modeling algorithm based on Biot's theory to generate the synthetic seismograms (CARCIONE and HELLE, 1999). The equations are expressed in the particle velocity-stress formulation. Viscoelasticity is introduced into Biot's poro-elastic equations (BIOT, 1962) for modeling a variety of dissipation mechanisms related to the matrix-fluid interaction. One of these mechanisms is the mesoscopic loss described by White's model (WHITE, 1975; CARCIONE *et al.*, 2003a,b; PRIDE *et al.*, 2004). Skeleton-fluid mechanisms are modeled by generalizing the coupling modulus M (see equation (52)) to a time-dependent relaxation function.

Let us denote by τ the total stress components, by p the (incremental) fluid pressure, by v and q the solid and fluid (relative to the solid) particle velocities, and by s the external sources of stress (body forces). Let us define the (dry-rock) P-wave modulus

$$E = K_m + \frac{4}{3}\mu_m, \tag{61}$$

and the composite dilatation field

$$\epsilon = \alpha(v_{x,x} + v_{z,z}) + q_{x,x} + q_{z,z}, \tag{62}$$

where the subscript "x,x" denotes $\partial/\partial x$.

The constitutive equations for an inhomogeneous, isotropic and poro-viscoelastic medium under plane-strain conditions are then given by
i) Biot-Euler's dynamical equations:

$$\tau_{xx,x} + \tau_{xz,z} = \rho v_{x,t} + \rho_f q_{x,t}, \tag{63}$$

$$\tau_{xz,x} + \tau_{zz,z} = \rho v_{z,t} + \rho_f q_{z,t}. \tag{64}$$

ii) Dynamic Darcy's law:

$$-p_{,x} = \rho_f v_{x,t} + m q_{x,t} + \frac{\eta_f}{\kappa} q_x, \tag{65}$$

and

$$-p_{,z} = \rho_f v_{z,t} + m q_{z,t} + \frac{\eta_f}{\kappa} q_z, \tag{66}$$

where $m = T\rho_f/\phi$, with T the tortuosity and κ the permeability of the medium.
iii) Constitutive equations:

$$\tau_{xx,t} = E v_{x,x} + (E - 2\mu_m) v_{z,z} + \alpha\left(M\epsilon + \sum_{l=1}^{L} e_l\right) + s_x, \tag{67}$$

$$\tau_{zz,t} = (E - 2\mu_m) v_{x,x} + E v_{z,z} + \alpha\left(M\epsilon + \sum_{l=1}^{L} e_l\right) + s_z, \tag{68}$$

$$\tau_{xz,t} = \mu_m(v_{x,z} + v_{z,x}) + s_{xz} \tag{69}$$

and

$$p_{,t} = -\left(M\epsilon + \sum_{l=1}^{L} e_l\right) + s_f, \tag{70}$$

where $e_l,\ l = 1, \ldots, L$ are memory variables.

iv) Memory variable equations:

$$e_{l,t} = -\frac{1}{\tau_{\sigma l}}\left[M\left(L + \sum_{m=1}^{L}\varphi_m\right)^{-1}\varphi_l\epsilon + e_l\right], \tag{71}$$

for $l = 1, \ldots, L$. where $\tau_{\epsilon l}$ and $\tau_{\sigma l}$ are sets of relaxation times, L is the number of attenuation mechanisms and

$$\varphi_l = \frac{\tau_{\epsilon l}}{\tau_{\sigma l}} - 1. \tag{72}$$

The P-wave attenuation and velocity (the relaxation times and parameter e in equation (27), respectively) are quantified by using White's model (see next section). An extension of the poroelastic code to the anisotropic case is available (CARCIONE, 1996), which can be useful to model effective (fine-layering), stress-induced (compaction) and crack- or fracture-induced anisotropy. The inclusion of S-wave attenuation can be performed by generalizing the shear modulus to a time-dependent relaxation function (CARCIONE *et al.*, 2004).

The computation of the spatial derivatives is performed with the staggered pseudo-spectral technique, which is noise-free in the dynamic range where regular grids generate artifacts that may have amplitudes similar to those of physical arrivals.

Physical Properties of CO_2 Bearing Rocks

Using the van der Waals equation (3), we compute the sound velocity and acoustic impedance of carbon dioxide and methane. The results are shown in Figure 2. Methane has a higher sound velocity than carbon dioxide although the impedance is lower for all pressures. This is due to the lower density of CH_4. Below the critical pressure (7.4 MPa), carbon dioxide is a gas. Sound velocity alone cannot discriminate between gas and liquid in the pressure range [0,15] MPa; an evaluation of the density is needed. Figure 3 shows the sound velocity (a) and acoustic impedance (b) of brine and oil as a function of pressure. The variations are opposite.

Figure 4 shows the sound velocity (a) and acoustic impedance (b) for the brine-CO_2 and oil-CO_2 mixtures as a function of the injected (initial) gas saturation S_g. The depth is 800 m. The same plot for a depth of 3 km is represented in Figure 5. In both cases, Wood's equation (26) is used to obtain the bulk modulus of the mixtures. The critical saturation for oil (53% in Figure 4 and 67% in Figure 5) is considerably higher than that of brine, which is approximately 1%. Below the critical saturation there is no free gas, and the mixture behaves as a liquid. Above the critical saturation, a small amount of free gas implies a sudden drop in the velocity of the liquid-gas mixture. This effect is less pronounced at 3 km. Figure 6 shows the same properties of Figure 4 under the same conditions but using equation (27) to obtain the bulk

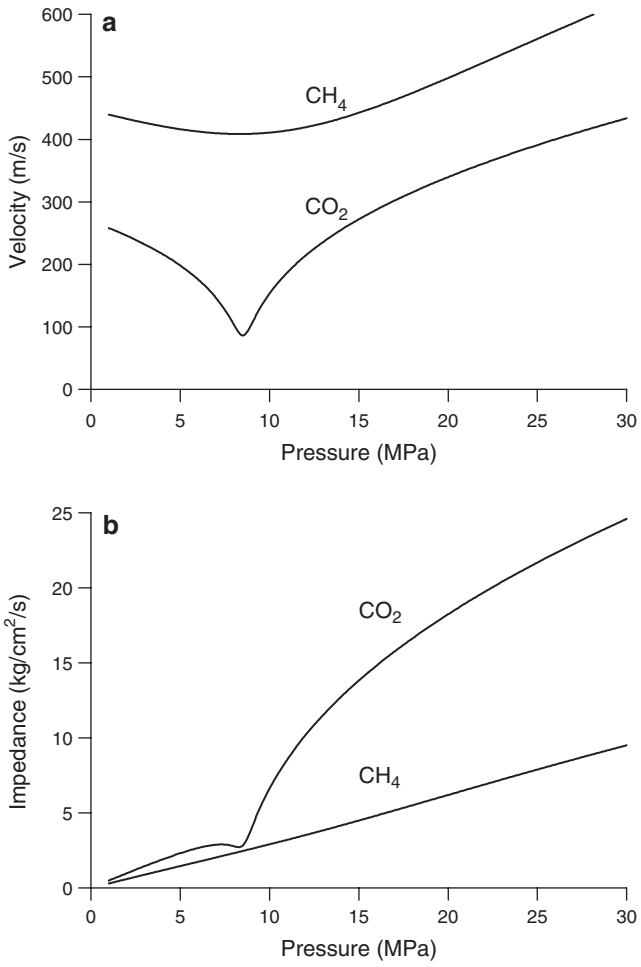

Figure 2
Sound velocity (a) and acoustic impedance (b) for carbon dioxide (CO_2) and methane (CH_4) as a function of pressure. Temperature and pressure are related by equations (1) and (2), with $\rho_w = 1.04$ g/cm^3, $G = 30$°C/km and $T_0 = 15$°C.

modulus of the liquid-gas mixture. This model predicts higher velocities beyond the critical saturation, in agreement with experimental data (CADORET *et al.*, 1995 (lime stones); KING *et al.*, 2000 (sand stones)).

Let us now consider the Utsira sand of the North Sea (ARTS *et al.*, 2004). A typical sample has a porosity of 36% and contains 70% quartz, 10% feldspar, 5% mica, 5% calcite, 5% clay and 5% illite. Using the average of the Hashin-Shtrikman bounds (34), we obtain the mineral moduli $K_s = 40$ GPa and $\mu_s = 38$ GPa, while the density is $\rho_s = 2600$ kg/m^3. For $z = 850$ m, $p = 10.7$ MPa, $p_c = 18$ MPa and

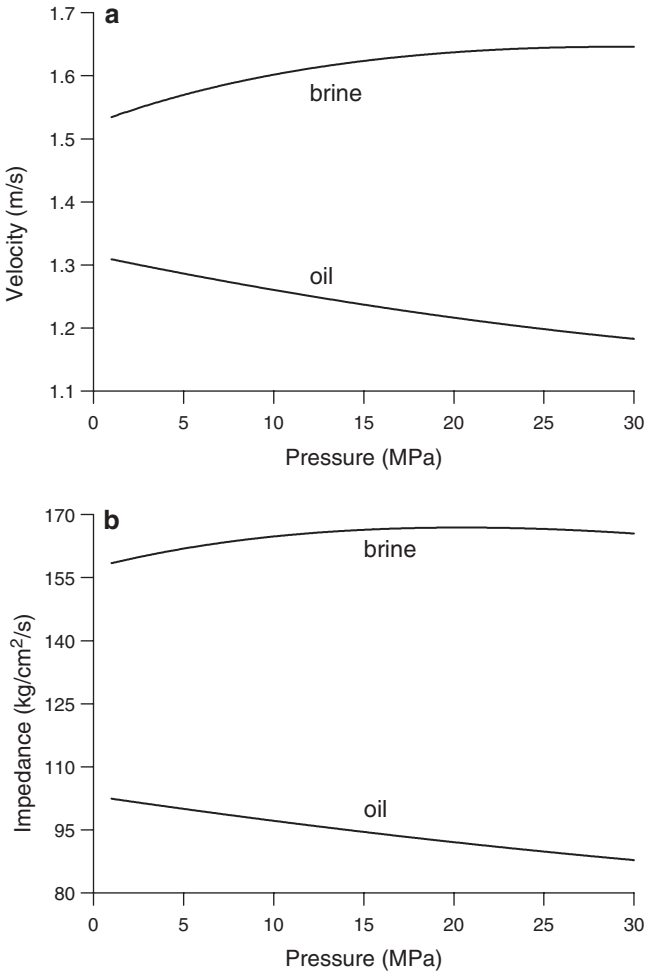

Figure 3
Sound velocity (a) and acoustic impedance (b) for brine and oil as a function of pressure. Temperature and pressure are related by equations (1) and (2), with $\rho_w = 1.04$ g/cm^3, $G = 30$°C/km and $T_0 = 15$°C. Moreover, $S = 50000$ ppm and API gravity = 50.

$T = 37$°C, the CO_2 properties are $\rho_g = 505$ kg/m^3 and $K_g = 0.025$ GPa, and the brine properties (without dissolved gas) are $\rho_B = 1032$ kg/m^3 and $K_B = 2.61$ GPa. To compute the matrix moduli of the Utsira sand, we use a critical porosity $\phi_c = 0.41$, Walton's "smooth" model (equations (43) and (45)), and the modified Hashin-Shtrikman lower bound (equations (49) and (50)), because the rock is unconsolidated; we obtain $K_m = 1.37$ GPa and $\mu = 0.82$ GPa, giving dry-rock P- and S-wave velocities of 1220 m/s and 704 m/s, respectively. To quantify the exponent e in

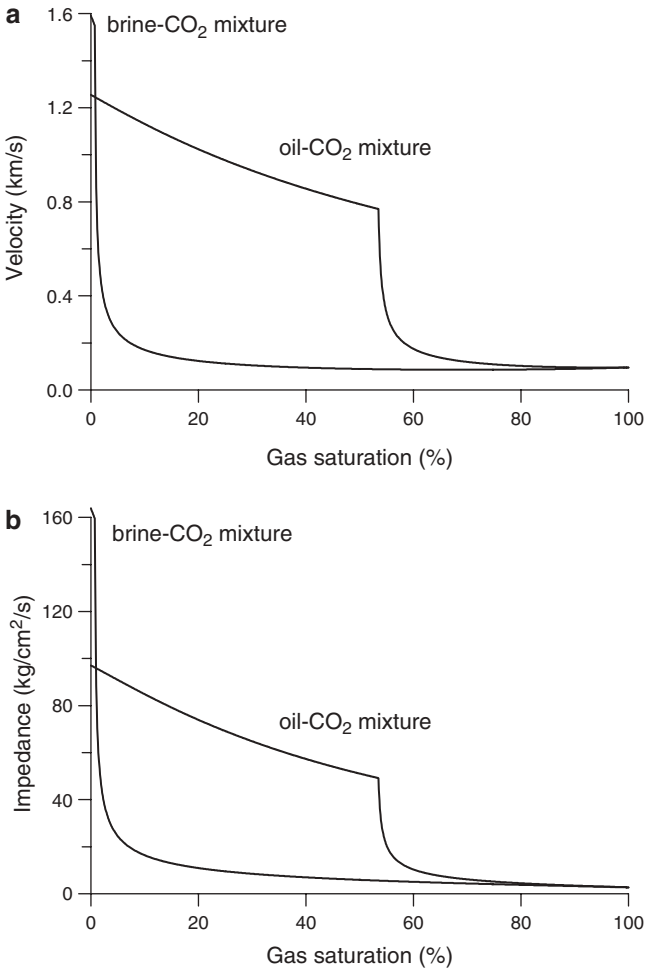

Figure 4
Sound velocity (a) and acoustic impedance (b) for the brine-CO_2 and oil-CO_2 mixtures as a function of the injected (initial) gas saturation S_g. The depth is 800 m, the temperature is 39°C and the pressure is 8 MPa. Moreover, $G = 30$°C/km, $T_0 = 15$°C, $S = 50000$ ppm and API gravity $= 50$.

equation (27) and the quality factor, we use White's model of patchy saturation (see Appendix A), with $b = 0.1$ m (size of the patches), $f = 30$ Hz, $\eta_1 = 0.0012$ Pa s, $\eta_2 = 0.00002$ Pa s, and $\kappa = 1.6$ D. A summary of the various properties that characterize the sand is given in Table 2.

Figure 7 shows the P-wave velocity (a) and dissipation factor (b) versus brine saturation of the sand filled with brine and CO_2. These properties have been obtained by using White's model and Wood's formula (26) to calculate the modulus of the

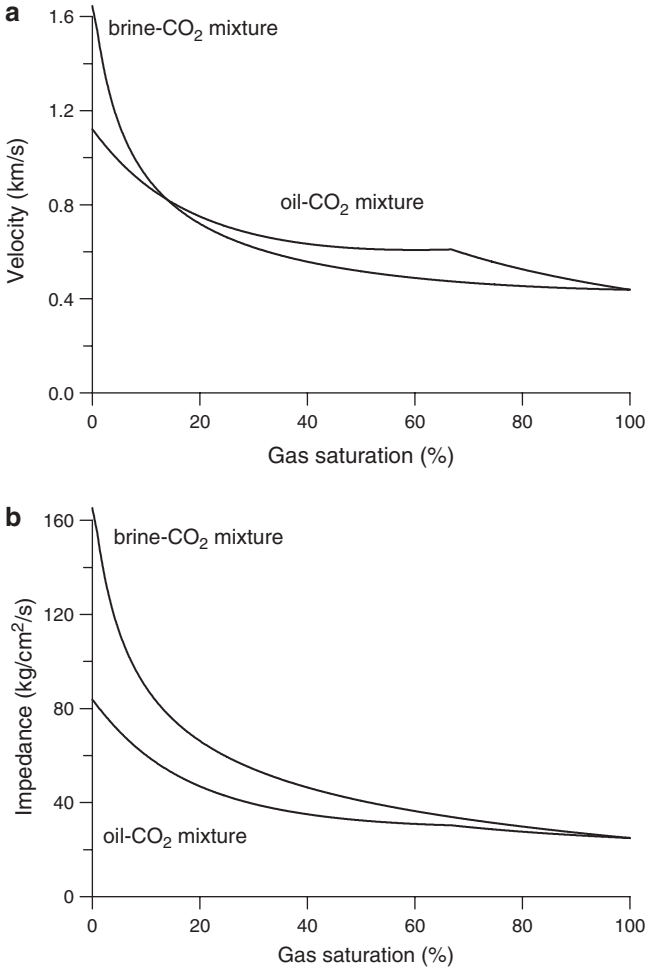

Figure 5
Sound velocity (a) and acoustic impedance (b) for the brine-CO_2 and oil-CO_2 mixtures as a function of the injected (initial) gas saturation. The depth is 3000 m, the temperature is 105°C and the pressure is 30 MPa. Moreover, $G = 30$°C/km, $T_0 = 15$°C, $S = 50000$ ppm and API gravity = 50.

pore-fluid mixture (curve denotes as Gassmann). The dotted curve corresponds to Brie's equation (27) with $e = 5$, which provides a fairly good fit to White's curve. The attenuation, due to mesoscopic loss, is significant due to the characteristics of the Utsira sand, i.e, high porosity, high permeability and low frame moduli. The S-wave velocity (a) and density (b) of the Utsira sand as a function of brine saturation is shown in Figure 8. The variation of the shear velocity is due to a density effect, since the wet-rock shear modulus is equal to the dry-rock shear modulus. The corresponding results for the Utsira sand partially saturated with oil and CO_2 are

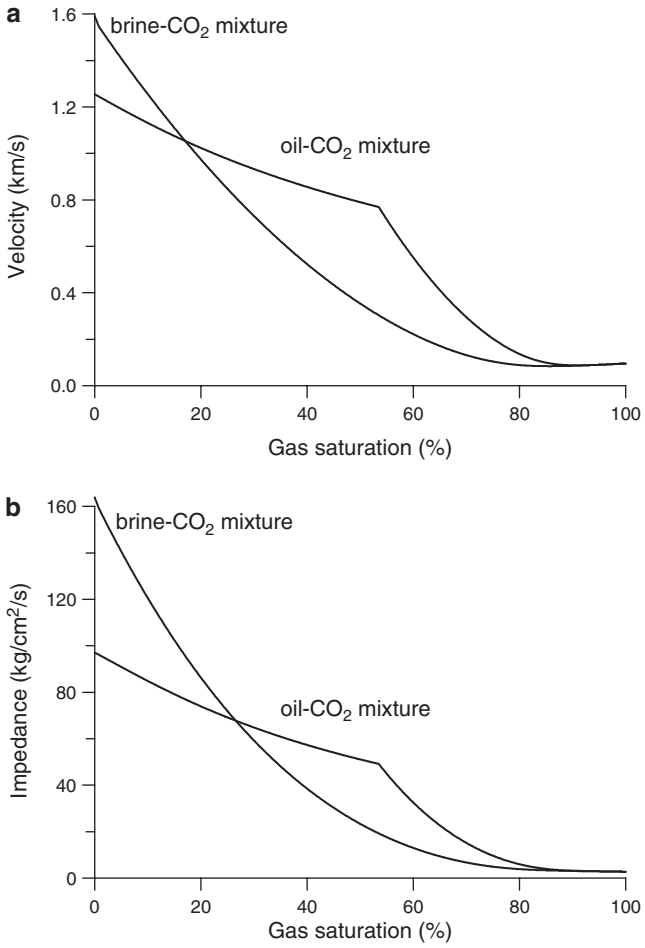

Figure 6
The same as in Figure 4, but using the Brie equation (27) with $e = 5$ (patchy saturation) to obtain the bulk modulus of the liquid-gas mixture beyond the critical saturation S_g.

shown in Figures 9 and 10. In this case $e = 1.2$ is used to fit White's curve. The critical saturation is approximately 50%; below this value the pore fluid is a mixture of gas and liquid. For comparsion, Figure 11 shows the same properties of Figure 9, but with CH_4 instead of CO_2. In this case, we take $e = 1.6$. As can be seen, the velocity and the dissipation factor of the P wave are higher. On the other hand, because the density of CH_4 is considerably lower than the CO_2 density, the shear-wave velocity is higher below the critical gas saturation (plot not shown). These differences, together with those of the P wave (nearly 100 m/s for velocity and a factor of 3 for the dissipation factor) indicate that, at least for shallow depths, it is

Table 2
Material properties of the Utsira sand (z = 850 m, p = 10 MPa, T = 37°C)

Grain bulk modulus, K_s	40 GPa
shear modulus, μ_s	38 GPa
density, ρ_s	2600 kg/m^3
Frame bulk modulus, K_m	1.37 GPa
shear modulus, μ_m	0.82 GPa
porosity, ϕ	0.36
permeability, κ	1.6 D
tortuosity, T	2.8
Brine density, ρ_B	1032 kg/m^3
viscosity, η_B	0.0012 Pa s
bulk modulus, K_B	2.61 GPa
Oil density, ρ_o	776 kg/m^3
viscosity, η_o	0.1 Pa s
bulk modulus, K_o	1.29 GPa
CH_4 density, ρ_g	79 kg/m^3
viscosity, η_g	0.0001 Pa s
bulk modulus, K_g	12.7 MPa
CO_2 density, ρ_g	505 kg/m^3
viscosity, η_g	0.00015 Pa s
bulk modulus, K_g	25 MPa

possible to distinguish between CO_2 and CH_4 saturated zones when the background fluid is oil. In the case of brine, the differences are less.

Synthetic Seismograms

We consider an idealized geometrical and physical model of the Utsira formation, with the purpose of illustrating the amplitude changes due to saturation differences within the Utsira sand only, although the modeling methodology can be used to describe any value of the physical properties at every cell of the mesh. The geological model is given in Figure 12 (e.g., EIKEN *et al.*, 2001). The numbers correspond to the properties shown in Table 3 (number 3 is the Utsira sand). The presence of thin shale layers (number 4) is the cause of different saturation values at different depths. We consider one relaxation mechanism, whose relaxation times are obtained as

$$\tau_\epsilon = \frac{\tau_0}{Q}\left(\sqrt{Q^2+1}+1\right) \quad \text{and} \quad \tau_\sigma = \frac{\tau_0}{Q}\left(\sqrt{Q^2+1}-1\right), \tag{73}$$

where $\tau_0 = 1/(2\pi f_0)$, and f_0 is the center frequency of the relaxation peak, which is taken here equal to the source dominant frequency.

The staggered grid has 300×360 points, with a grid spacing of 5 m, and the source is a Ricker-type wavelet with a dominant frequency of 50 Hz. Figure 13 shows the synthetic seismic sections with 100% brine saturation (a) (before injection, with the Utsira formation fully saturated with brine), with partial saturation (b) (as shown

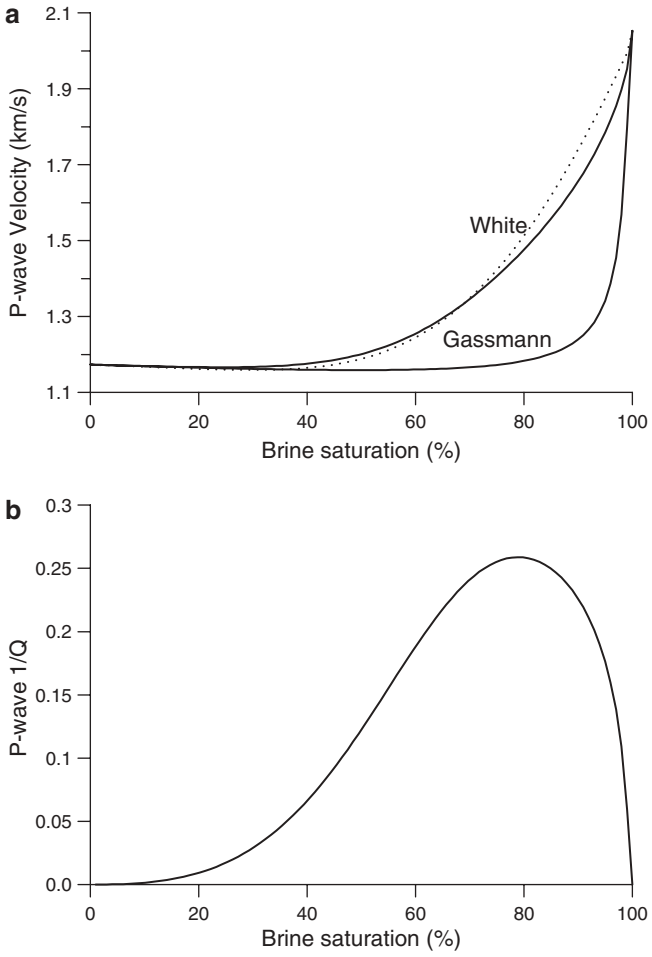

Figure 7
P-wave velocity (a) and dissipation factor (b) of the Utsira sand versus brine saturation, obtained with White's model and using Wood's formula (26) to describe the modulus of the CO_2-brine mixture (curve denote as Gassmann). The dotted curve corresponds to Brie's equation (27), with $e = 5$. The quality factor, predicted by White's model, is computed at 30 Hz.

in Fig. 12) and the difference section (c). Figure 13d shows the the post-injection seismogram obtained without attenuation. The main reflections in Figure 13a arise from the top and bottom of the Utsira formation and from the embedded shale layers. The events are enhanced when the formation is partially saturated with CO_2 (b), showing that the difference section (c) reveals the presence of the CO_2, in agreement with the features observed in the real data (EIKEN *et al.*, 2001; CHADWICK *et al.*, 2002). Figure 13d indicates that modeling the poroelastic effects and

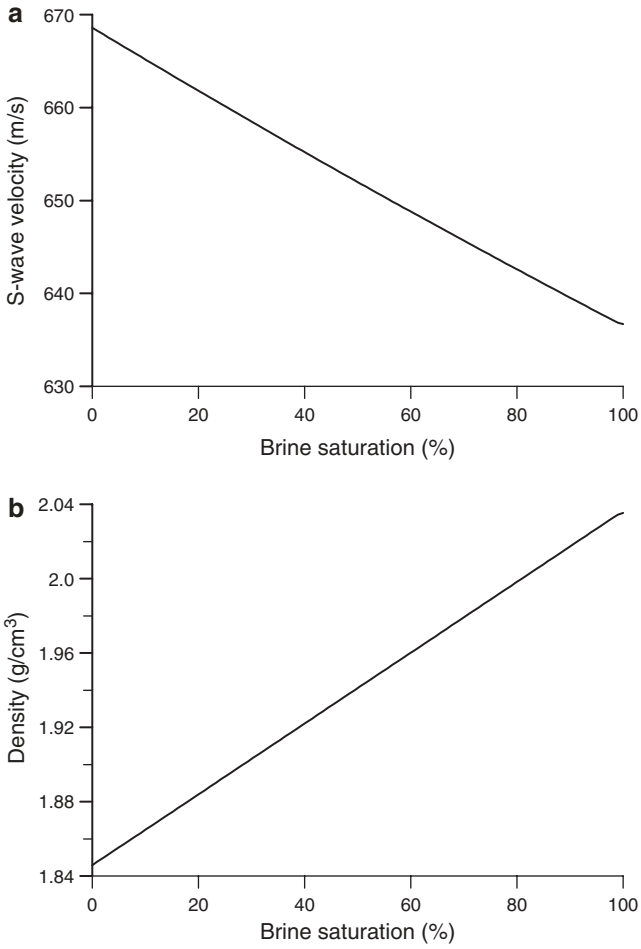

Figure 8
S-wave velocity (a) and density (b) of the Utsira sand partially saturated with CO_2 versus brine saturation.

attenuation is important, since the amplitude differences with the seismogram of Figure 13b are significant.

Conclusions

Time-lapse seismic technology is essential to detect and monitor the presence of CO_2 in geological formations. The success of the monitoring is subject to a correct description of the physical properties of the CO_2 bearing rocks. Using the petrophysical model developed in this work, we conclude the following: 1. Methane has a higher sound velocity than carbon dioxide however the impedance is lower for all

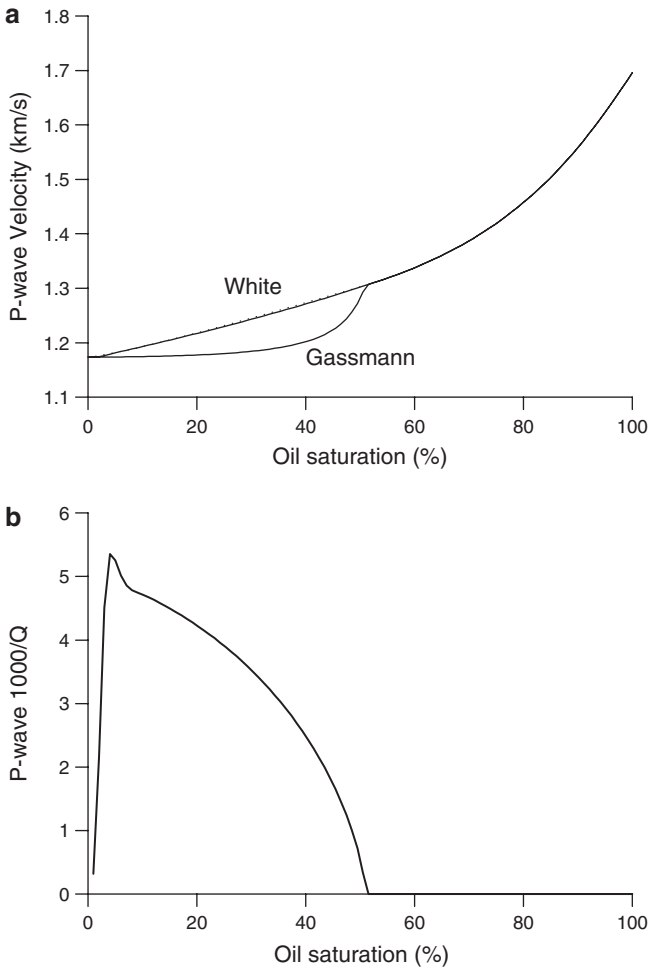

Figure 9
P-wave velocity (a) and dissipation factor (b) of the Utsira sand versus oil saturation, obtained with White's model and using Wood's formula (26) to describe the modulus of the CO_2-oil mixture (curve denote as Gassmann). The dotted curve corresponds to Brie's equation (27), with $e = 1.2$. The quality factor, predicted by White's model, is computed at 30 Hz.

pressures. This is due to the lower density of CH_4. Sound velocity alone cannot discriminate between gas and liquid CO_2 in the pressure range [0,15] MPa; an evaluation of the density is needed. 2. The sound velocity and acoustic impedance of brine increases with increasing pore pressure. Oil shows the opposite behavior. 3. The sound velocity and acoustic impedance of the brine-CO_2 and oil-CO_2 mixtures as a function of the injected (initial) gas saturation display very dissimilar behaviors at shallow depths resulting because the critical saturation of oil is considerably higher than the critical saturation of brine (below the critical saturation there is no free gas,

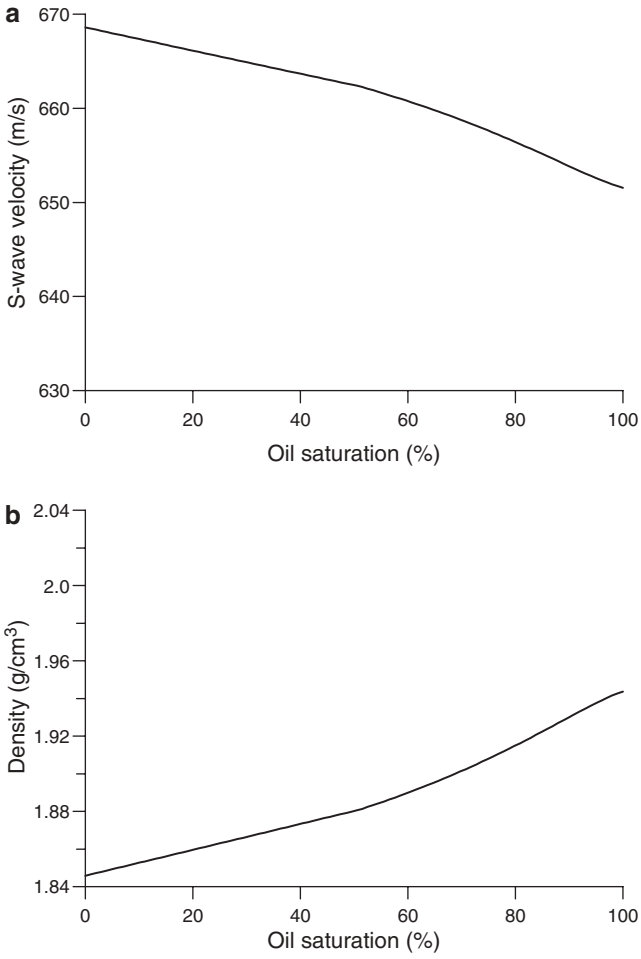

Figure 10
S-wave velocity (a) and density (b) of the Utsira sand partially saturated with CO_2 versus oil saturation.

and the mixture behaves as a liquid). Beyond the critical saturation, a small amount of free gas implies a sudden drop in the velocity of the liquid-gas mixture. This effect is less pronounced at deeper depths. 4. For patchy saturation, the model predicts higher velocities beyond the critical saturation.

The calculations for the shallow Utsira aquifer of the North Sea reveal that: 1. The P-wave velocity discriminates between uniform and patchy saturation for brine saturations above 60%. 2. The attenuation due to mesoscopic loss peaks at 80% brine saturation. 3. The S-wave velocity decreases and the density increases with increasing brine saturation. 4. The P-wave velocity discriminates between uniform and patchy saturation for oil saturations between nearly 20 and 50%. 5. The attenuation due to mesoscopic loss peaks at 5% oil saturation. 6. It is possible to

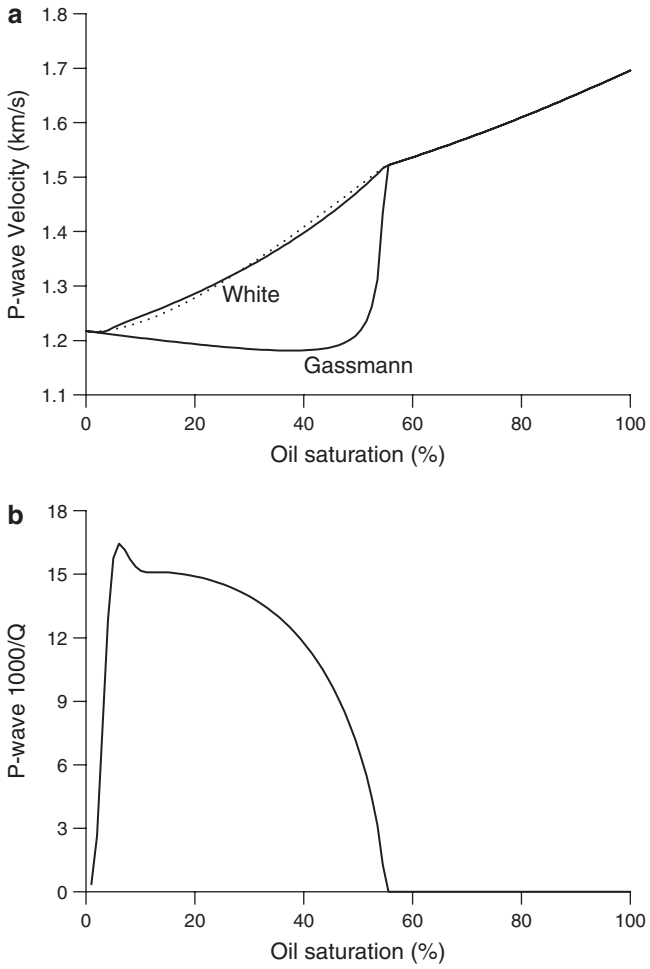

Figure 11
P-wave velocity (a) and dissipation factor (b) of the Utsira sand versus oil saturation, obtained with White's model and using Wood's formula (26) to describe the modulus of the CH_4-oil mixture (curve denote as Gassmann). The dotted curve corresponds to Brie's equation (27), with $e = 1.6$. The quality factor, predicted by White's model, is computed at 30 Hz.

distinguish between CO_2 and CH_4 saturated zones when the background fluid is oil. In the case of brine, the differences are smaller.

The poro-viscoelastic seismograms before and after CO_2 injection show the expected differences compared to the real data. Use of the present methodology allows our direct control of the reservoir properties, such as, dry-rock moduli, porosity, permeability and fluid properties, and *in situ* conditions such as pore pressure and temperature.

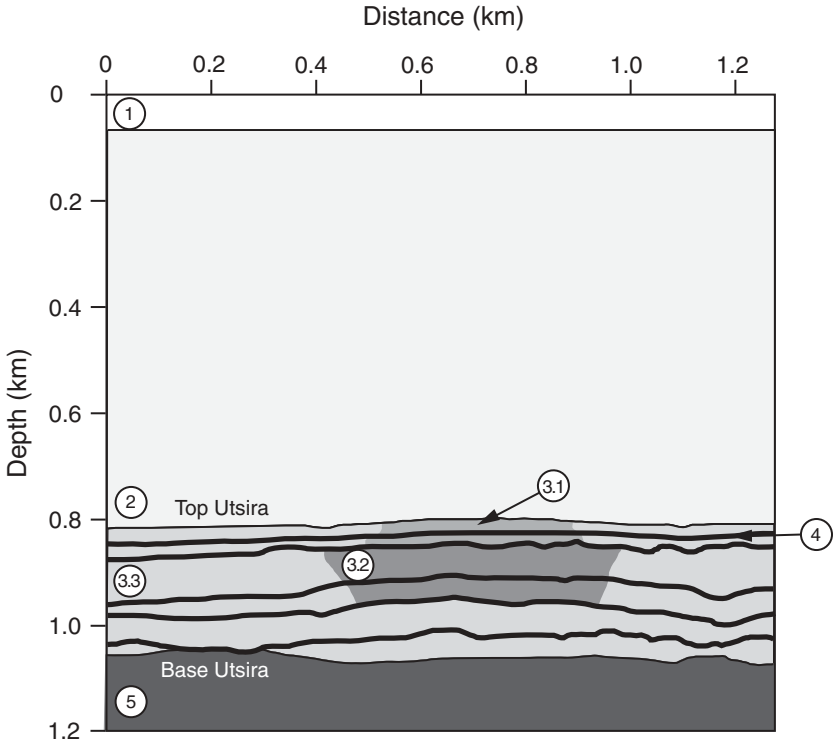

Figure 12
Cross section of the geological model. The numbers correspond to the material properties indicated in Table 3.

Appendix A-White's model

WHITE (1975) assumed spherical patches considerably larger than the grains but much smaller than the wavelength. He developed the theory for a gas-filled sphere of porous medium of radius a located inside a water-filled sphere of porous medium of outer radius b ($a < b$). Let us denote the saturation of gas and water by S_1 and S_2, respectively. Then

$$S_1 = \frac{a^3}{b^3}, \quad S_2 = 1 - S_1. \tag{A-1}$$

The complex P-wave velocity is given by

$$V_c = \sqrt{\frac{K + 4\mu_m/3}{\rho}}, \tag{A-2}$$

Table 3
Poro-viscoelastic properties of the Utsira-aquifer model

Medium	ρ_s (kg/m^3)	K_s (GPa)	ϕ	K_m (GPa)	μ_m (GPa)	T	η_f (cP)	κ (Darcy)	ρ_f (kg/m^3)	K_f (GPa)	Q	V_P (km/s)	V_S (km/s)	ρ (kg/m^3)
1	0	0	1	0	0	1	1.2	100	1030	2.25	10000	1.48	0	1030
2	2600	20	0.32	1.50	0.73	4	1.2	0.1	1030	2.25	60	1.88	0.583	2097
3.1[a]	2600	40	0.35	1.33	0.85	2.8	0.3	1.6	715	0.042	15	1.15	0.661	1940
3.2[b]	2600	40	0.35	1.33	0.85	2.8	0.7	1.6	935	0.12	5	1.17	0.649	2017
3.3[c]	2600	40	0.35	1.33	0.85	2.8	1.2	1.6	1032	2.61	100	2.06	0.644	2051
4	2600	20	0.25	4.70	0.99	5	1.2	0.001	1030	2.25	80	2.16	0.670	2207
5	2600	20	0.2	6.49	1.16	5	1.2	0.01	1030	2.25	100	2.3	0.712	2286

a: $S_w = 40\%$; b: $S_w = 80\%$; c: $S_w = 100\%$.

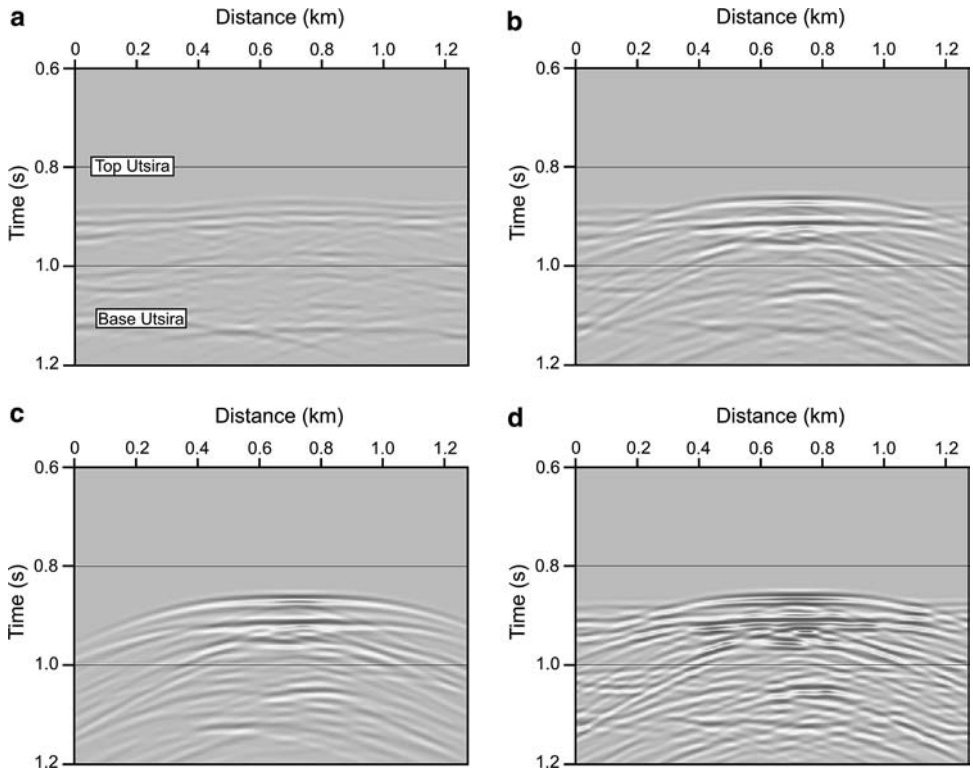

Figure 13
Synthetic seismic sections with 100% brine saturation (before injection) (a), partial saturation (as shown in Figure 12) (b), and difference section (c). Figure (d) depicts the seismogram with partial saturation and without attenuation.

where K is the complex bulk modulus (given below), μ_m is the dry-rock shear modulus, $\rho = (1-\phi)\rho_s + \phi\rho_f$ is the bulk density, ρ_s is the grain density, and ϕ is the porosity. The density of the fluid mixture is

$$\rho_f = S_1\rho_{f1} + (1-S_1)\rho_{f2}, \tag{A-3}$$

where ρ_{f1} and ρ_{f2} are the densities of fluid 1 and fluid 2 (gas and water in White's theory).

Assuming that the dry-rock and grain moduli, and permeability, κ, of the different regions are the same, the complex bulk modulus as a function of frequency is given by

$$K = \frac{K_\infty}{1 - K_\infty W}, \tag{A-4}$$

where

$$
\begin{aligned}
W &= \frac{3ia\kappa(R_1 - R_2)}{b^3\omega(\eta_1 Z_1 - \eta_2 Z_2)}\left(\frac{K_{A1}}{K_1} - \frac{K_{A2}}{K_2}\right),\\
R_1 &= \frac{(K_1 - K_m)(3K_2 + 4\mu_m)}{K_2(3K_1 + 4\mu_m) + 4\mu_m(K_1 - K_2)S_1},\\
R_2 &= \frac{(K_2 - K_m)(3K_1 + 4\mu_m)}{K_2(3K_1 + 4\mu_m) + 4\mu_m(K_1 - K_2)S_1},\\
Z_1 &= \frac{1 - \exp(-2\gamma_1 a)}{(\gamma_1 a - 1) + (\gamma_1 a + 1)\exp(-2\gamma_1 a)},\\
Z_2 &= \frac{(\gamma_2 b + 1) + (\gamma_2 b - 1)\exp[2\gamma_2(b - a)]}{(\gamma_2 b + 1)(\gamma_2 a - 1) - (\gamma_2 b - 1)(\gamma_2 a + 1)\exp[2\gamma_2(b - a)]},\\
\gamma_j &= \sqrt{i\omega\eta_j/(\kappa K_{Ej})},\\
K_{Ej} &= \left[1 - \frac{\alpha K_{fj}(1 - K_j/K_s)}{\phi K_j(1 - K_{fj}/K_s)}\right]K_{Aj},\\
K_{Aj} &= \left[\frac{\phi}{K_{fj}} + \frac{1}{K_s}(\alpha - \phi)\right]^{-1}, \quad j = 1, 2,\\
\alpha &= 1 - \frac{K_m}{K_s},
\end{aligned}
\tag{A-5}
$$

K_s is the bulk modulus of the grains, K_{fj} are the bulk moduli of the fluids, η_j are the fluid viscosities, and

$$
K_\infty = \frac{K_2(3K_1 + 4\mu_m) + 4\mu_m(K_1 - K_2)S_1}{(3K_1 + 4\mu_m) - 3(K_1 - K_2)S_1} \tag{A-6}
$$

is the — high frequency — bulk modulus when there is no fluid flow between the patches. K_1 and K_2 are the — low frequency — Gassmann moduli which are given by

$$
K_j = \frac{K_s - K_m + \phi K_m\left(K_s/K_{fj} - 1\right)}{1 - \phi - K_m/K_s + \phi K_s/K_{fj}}, \quad j = 1, 2, \tag{A-7}
$$

where K_m is the dry-rock bulk modulus.

We should be aware of the limitations of the theory. For simplicity in the calculations, White considers an outer sphere of radius b ($b > a$), instead of a cube. Thus, the system consists of two concentric spheres, in which the volume of the outer sphere is the same as the volume of the original cube. The outer radius is $b = l/(4\pi/3)^{1/3}$, where l is the size of the cube. The distance between pockets is l. When $a = l/2$ the gas pockets touch each other. This happens when $S_1 = \pi/6 = 0.52$. Therefore, for values of the gas saturation higher than these critical value, or values of the water saturation between 0 and 0.48, the theory is not rigorously valid. Another limitation to consider is that the size of gas pockets should be decidedly smaller than the wavelength, i.e., $a \ll c_r/f$, where c_r is a reference velocity and f is the frequency.

References

Arts, R., Eiken, O., Chadwick, R.A., Zweigel, P., Van der meer, L., and Zinszner, B. (2004), *Monitoring of CO_2 injected at Sleipner using time-lapse seismic data*, Energy *29*, 1383–1392.

Athy, L.F. (1930), *Density porosity, and compaction of sedimentary rocks*, Bull. Am. Assoc. Petro. Geologists *14*, 1–24.

Batzle, M. and Wang, Z. (1992), *Seismic properties of pore fluids*, Geophysics *57*, 1396–1408.

Biot, M.A. (1962), *Mechanics of deformation and acoustic propagation in porous media*, J. Appl. Phys. *33*, 1482–1498.

Brie, A., Pampuri, F., Marsala, A.F., and Meazza, O. (1995), *Shear sonic interpretation in gas-bearing sands*, SPE Annual Technical Conf., nr. 30595, pp. 701–710.

Cadoret, T., Marion, D., and Zinszner, B. (1995), *Influence of frequency and fluid distribution on elastic wave velocities in partially saturated limestones*, J. Geophys. Res. *100*, 9789–9803.

Carcione, J.M. (1996), *Wave propagation in anisotropic, saturated porous media: plane wave theory and numerical simulation*, J. Acous. Soc. Am. *99*(5), 2655–2666.

Carcione, J.M., *Wavefields in real media: Wave propagation in anisotropic, anelastic and porous media*. In *Handbook of Geophysical Exploration*, vol. 31, (Pergamon Press Inc., 2001).

Carcione, J.M., Cavallini, F., Santos, J.E., Ravazzoli, C.L., and Gauzellino, P.M. (2004), *Wave propagation in partially-saturated porous media: Simulation of a second slow wave*, Wave Motion *39*, 227–240.

Carcione, J.M. and Gangi, A. (2000), *Gas generation and overpressure: Effects on seismic attributes*, Geophysics *65*, 1769–1779.

Carcione, J.M. and Helle, H.B. (1999), *Numerical solution of the poroviscoelastic wave equation on a staggered mesh*, J. Comput. Phys. *154*(2), 520–527.

Carcione, J.M., Helle, H.B., and Pham, N.H. (2003a), *White's model for wave propagation in partially saturated rocks: Comparison with poroelastic numerical experiments*, Geophysics *68*, 1389–1398.

Carcione, J.M., Helle, H.B., Santos, J.E., and Ravazzoli, C.L. (2005), *A generalized Gassmann modulus for multi-mineral porous media*, Geophysics *70*, N17–N26.

Carcione, J.M., Seriani, G., and Gei, D. (2003b), *Acoustic and electromagnetic properties of soils saturated with salt water and NAPL*, J. Appl. Geophys. *52*, 177–191.

Carcione, J.M. and Tinivella, U. (2001), *The seismic response to overpressure: A modeling methodology based on laboratory, well and seismic data*, Geophys. Prosp. *49*, 523–539.

Chadwick, R.A., Zweigel, P., Gregersen, U., Kirby, G.A., Holloway, G.A.S., and Johannssen, P.N. (2002), *Geological Characterisation of CO_2 storage sites: Lessons from Sleipner, Northern North Sea*, 6th International Conference on Greenhouse Gas Control Technology, Kyoto, Japan, expanded abstract.

Dodson, C.R. and Standing, M.B. (1945), *Pressure-volume-temperature and solubility relations for natural-gas-water mixtures*. In *Drilling and Production Practices*, Am. Petr. Inst.

Dvorkin, J. and Nur, A. (1996), *Elasticity of high-porosity sandstones: Theory for two North Sea data sets*, Geophysics *61*, 1363–1370.

Eiken, O., Brevik, I., Arts, R., Lindeberg, E., and Fagervik, K. (2001), *Seismic monitoring of CO_2 injected into a marine acquifer*, AAPG, Annual Meeting, Denver, USA, expanded abstract.

Færseth, R.B. (1996), *Interaction of Permo-Triassic and Jurassic extensional fault-blocks during the development of the Northern Sea*, J. Geol. Soc. London *153*, 931–944.

Friedman, A.S., *Pressure-volume-temperature relationships of gases, virial coefficients*. In *American Institute of Physics Handbook* (New York, McGraw-Hill Book Co 1963).

Gei, D. and Carcione, J.M. (2003), *Acoustic properties of sediments saturated with gas hydrate, free gas and water*, Geophys. Prosp. *51*, 141–157.

Hashin, Z. and Shtrikman, S. (1963), *A variational approach to the theory of the elastic behaviour of multiphase materials*, J. Mech. Phys. Sol. *11*, 127–140.

Hoversten, G.M., Gritto, R., Washbourne, J., and Daley, T. (2003), *Pressure and fluid saturation prediction in a multicomponent reservoir using combined seismic and electromagnetic imaging*, Geophysics *68*, 1580–1591.

Kaszuba, J.P., Janecky, D.R., and Snow, M.G. (2003), *Carbon dioxide reaction processes in a model brine aquifer at 200°C and 200 bars: Implications for geologic sequestration of carbon*, Appl. Geochem. *18*, 1065–1080.

KASELOW, A. and SHAPIRO, S.A. (2004), *Stress sensitivity of elastic moduli and electrical resistivity in porous rocks*, J. Geophys. Eng. *1*, 1–11.

KING, M.S., MARSDEN, J.R., and DENNIS, J.W. (2000), *Biot dispersion for P- and S-waves velocities in partially and fully saturated sandstones*, Geophys. Prosp. *48*, 1075–1089.

LEDLEY, T.S., SUNDQUIST, E.T., SCHWARTZ, S.E., HALL, D.K., FELLOWS, J.D., and KILLEEN, T.L. (1999), *Climate Change and Greenhouse Gases*, EOS, Transaction Am. Geoph. Union, *80*(39), 453–458.

MAVKO, G., MUKERJI, T., and DVORKIN, J., *The Rock Physics Handbook: Tools for Seismic Analysis in Porous Media* (Cambridge University Press, Cambridge, UK 1998).

MORSE, P.M. and INGARD, K.U., *Theoretical Acoustics* (Princeton University Press, Princeton, New Jersey 1986).

MURPHY, W.F. (1982), *Effects of microstructure and pore fluids on the acoustic properties of granular sedimentary materials*, Ph.D. Thesis, Stanford University.

OLDENBURG, C.M. (2003), C*arbon dioxide as cushion gas for natural gas storage*, Energy and Fuels *17*, 240–246.

PRASAD, M. and MANGHNANI, M.H. (1997), *Effects of pore and differential pressure on compressional wave velocity and quality factor in Berea and Michigan sandstones*, Geophysics *62*, 1163–1176.

PRIDE, S.R., BERRYMAN, J.G., and HARRIS, J.M. (2004), *Seismic attenuation due to wave-induced flow*, J. Geophys. Res. *109*, B01201, doi:10.1029/2003JB002639.

POLING, B.E., PRASUNITZ, J.M., and O'CONNEL, J.P., *The Properties of Gases and Liquids* McGraw-Hill Inc. 2001).

PREUSS, K., XU, Y., APPS, J., and GARCIA, J. (2001), *Numerical modeling of aquifer disposal of CO2*, SPE/EPA/DOE Exploration and Production Environmental Conference, SPE 66537.

SPAN, R. and WAGNER, W. (1996), *A new equation of state for carbon dioxide covering the fluid region from the triple-point temperature to 100 K at pressures up to 800 MPa*, Phys. Chem. Ref. Data *25*, 1509–1596.

STANDING, M.B., *Volumetric and Phase Behavior of Oil Field Hydrocarbon Systems* (New York, N. Y., Reinhold Publishing Corp. 1952).

TEJA, A.S. and RICE, P. (1981), *Generalized corresponding states method for viscosities of liquid mixtures*. In *Ind. Eng. Chem. Fundamentals*, vol. 20, pp. 77–81.

XUE, Z. and OHSUMI, T. (2004), *Seismic wave monitoring of CO_2 migration in water-saturated porous sandstone*, Exploration Geophysics *35*, 25–32.

WALTON, K. (1987), *The effective elatic moduli of a random packing of spheres*, J. Mech. Phys. Sol. *35*, 213–226.

WANG, Z., CATES, M., and LANGAN, R.T. (1998), *Seismic monitoring of a CO_2 flood in a carbonate reservoir: A rock physics study*, Geophysics *63*, 1604–1617.

WHITE, J.E. (1975), *Computed seismic speeds and attenuation in rocks with partial gas saturation*, Geophysics *40*, 224–232.

ZIMMERMAN, R.W., *Compressibility of Sandstones* (Elsevier Science Pub. Co. Inc. 1991).

(Received April 29, 2005; accepted August 3, 2005)